In-Crystal and Surface Charge Transport of Electric-Field-Induced Carriers in Organic Single-Crystal Semiconductors

J. Takeya,[1,*] J. Kato,[2,3] K. Hara,[1,2,3] M. Yamagishi,[1] R. Hirahara,[1] K. Yamada,[2] Y. Nakazawa,[1] S. Ikehata,[3] K. Tsukagoshi,[4,5] Y. Aoyagi,[4,6] T. Takenobu,[7,8] and Y. Iwasa[7,8]

[1]*Graduate School of Science, Osaka University, Toyonaka 560-0043, Japan*
[2]*Materials Science Research Laboratory, CRIEPI, Tokyo 201-8511, Japan*
[3]*Department of Physics, Tokyo University of Science, Tokyo 162-8601, Japan*
[4]*RIKEN, Hirosawa 2-1, Wako 351-0198, Japan*
[5]*PRESTO, Japan Science and Technology Agency, Kawaguchi 333-0012, Japan*
[6]*Tokyo Institute of Technology, Yokohama 336-8502, Japan*
[7]*Institute for Materials Research, Tohoku University, Sendai 980-8577, Japan*
[8]*CREST, Japan Science and Technology Agency, Kawaguchi 333-0012, Japan*
(Received 26 July 2006; published 9 May 2007)

Gate-voltage dependence of carrier mobility is measured in high-performance field-effect transistors of rubrene single crystals by simultaneous detection of the longitudinal conductivity $\sigma_\square$ and Hall coefficient R_H. The Hall mobility μ_H ($\equiv \sigma_\square R_H$) reaches nearly 10 $\mathrm{cm^2/V\,s}$ when relatively low-density carriers ($<10^{11}$ $\mathrm{cm^{-2}}$) distribute into the crystal. μ_H rapidly decreases with higher-density carriers as they are essentially confined to the surface and are subjected to randomness of the amorphous gate insulators. The mechanism to realize high carrier mobility in the organic transistor devices involves intrinsic-semiconductor character of the high-purity organic crystals and diffusive bandlike carrier transport in the bulk.

DOI: 10.1103/PhysRevLett.98.196804 PACS numbers: 73.40.−c, 72.80.Le, 73.61.Ph

Doped π-conjugated molecular semiconductors provide unique electronic systems with a relatively small intermolecular transfer integral (typically ≤ 0.5 eV) and significant coupling to molecular vibration, both of which play a major role even at ordinary temperatures. Simply, the two fundamental transport mechanisms would be a band transport with mass-enhanced carriers and a hopping transport with self-localized carriers in predominance of molecular reorganization energy [1]. The reality, however, has been argued to be in some complex competition between the two extreme cases, grounded on experimental and theoretical works introducing the ideas of ''polaronic band transport'' [2–5]. Though understanding the carrier transport in such ''soft'' semiconductor crystals is of emergent importance because of recent technological attention to organic flexible electronics, methods of experimental approaches are still under development toward a full description of the fundamental electronic states of the charge carriers.

A conventional method to evaluate carrier mobility μ in the *bulk* of organic semiconductors has been by the time-of-flight (TOF) measurement using photoinduced carriers accelerated by electric field [6,7]. Measuring the current of space-charge carriers in the organic semiconductor has been another approach to evaluate the bulk crystalline mobility: μ as high as $\sim$35 $\mathrm{cm^2/V\,s}$ was recently reported at room temperature with an ultrapure pentacene crystal [8]. On the other hand, gaining popularity these days is to measure the field-effect mobility μ_{FET}, accumulating carriers in the organic semiconductors by the application of gate electric field to the adjacent gate dielectric insulators. Since the induced carriers are attracted to the gate insulators by the electric field, this method is generally regarded as a surface-sensitive probe. Besides the direct relevance to the technology of the organic field-effect transistors (FETs), the method provides a dc transport property accessible to the lowest-energy physics at low temperatures [9], as well as the maximum carrier density one or two orders higher than achievable with the conventional techniques. Recently, development of organic single-crystal transistors enabled more fundamental evaluation of μ_{FET} without influences of grain boundaries [10–12], which would reduce carrier motion in polycrystalline thin-film transistors. Furthermore, owing to recent Hall-effect measurements, ''intrinsic'' Hall mobility μ_H is given for the single-crystal FETs by discriminating well-mobile carriers from narrowly hopping trapped charges [13,14]. It is, however, still questionable if μ_H is identical to the dc bulk mobility of the crystals, because the influences of the semiconductor-insulator boundary are not yet fully understood.

In this Letter, we present an experiment to introduce carriers inside the crystal *with the configuration of FETs*. Since the organic semiconductors are basically nondoped intrinsic semiconductors, the length scale of the carrier distribution can be elongated in a weak electric field with the use of purified single crystals in principle. Preparing nearly best performing organic single-crystal FETs, we show high-mobility transport of the *in-crystal* carriers for the first time by simultaneous measurement of sheet conductivity $\sigma_\square$ and Hall coefficient R_H; the high mobility of $\sim$10 $\mathrm{cm^2/V\,s}$ is achieved when the field-induced carriers rather dilutely distribute into the crystal at weak gate fields,

 © 2007 The American Physical Society

whereas the mobility rapidly decreases with increasing gate electric field, as the carriers are concentrated in the vicinity of the interface.

We construct the bottom-contact FETs by laminating thin rubrene crystals onto PVP/doped silicon substrates on which 10-nm thick gold electrodes are evaporated and patterned by means of photolithography [11,15]. To form the PVP gate insulator on the doped silicon wafers, a solution of poly-4-vinylphenol and polymelamine-co-formaldehyde in propylene glycol monomethyl ether acetate (PGMEA) is deposited by spin coating and cross-linked at 200 °C for 20 min. The typical thickness of the PVP layer is 1–5 μm. The single crystals typically less than 1 μm thick are grown by physical vapor transport to attach on the PVP substrates. Furthermore, the samples for the Hall-effect measurements are shaped into the "six-probe Hall-bar" using a laser etching equipment [16]. Source Measure Units of Agilent Technology E5270 semiconductor parameter analyzer are used to apply V_D and V_G, to measure I_D and gate leakage current I_G, and to measure voltages V_1, V_2, and V_3 at three points on the crystal, for the purpose of identifying longitudinal sheet conductivity $\sigma_\square$ $[= I_D/(V_2 - V_1)L_{12}/W]$ and transverse Hall voltage $V_3 - V_1$ in external magnetic field B perpendicular to the channel [the configuration will be illustrated in the inset of Fig. 1(d)]. L_{12} is the distance between the two voltage probes along the current direction and W is the channel width. All the measurements are carried out in the Ohmic regime where $\sigma_\square$ is independent of V_D.

Prior to the Hall-effect measurements, we have characterized the rubrene/PVP FETs by usual longitudinal conductivity measurements in zero magnetic field. Plotted in the main panel of Fig. 1(a) is drain current I_D as a function of V_G in the Ohmic regime ($V_D = -1$ V) for the sample that exhibited the highest mobility. The inset of Fig. 1(a) gives a top view of the sample. Hole conductivity switches on at the threshold gate voltage V_{th} and increases as holes are accumulated in the rubrene crystal with negative V_G application. For the above prepared rubrene/PVP FETs, it is a general trend that transconductance $g_m(V_G)$ $(\equiv \partial I_D/\partial V_G)$ is larger at V_G near V_{th} than at higher negative V_G. According to the well-known formula

$$\mu_{\text{FET}} = 1/C_i \partial\sigma_\square/\partial V_G, \tag{1}$$

grounded on

$$\sigma_\square = C_i(V_G - V_{\text{th}})\mu_{\text{FET}} \tag{2}$$

(we note that $\sigma_\square$ is given with the unit of S by integrating conductivity with respect to the distance from the surface of the crystal); mobility value μ_1 is evaluated to be in the range of 5–25 cm^2/V s near V_{th}, while $\mu_2 \sim$ 1–2 cm^2/V s at large negative gate voltages, depending on the samples. Two among the 20 samples show outstanding values of μ_1 exceeding 20 cm^2/V s.

Hall-effect measurements provide a direct estimate of the carrier density as a function of V_G in the high-mobility crystal FETs so that the microscopic mechanism can be elucidated of the rather unfamiliar transfer curves presented above. Noting that Eq. (1) is correct only when C_i is not dependent on V_G, it is necessary to examine whether or not the carriers are doped with the same rate with increasing V_G as $C_i(V_G - V_{\text{th}})$, i.e., whether anomalous

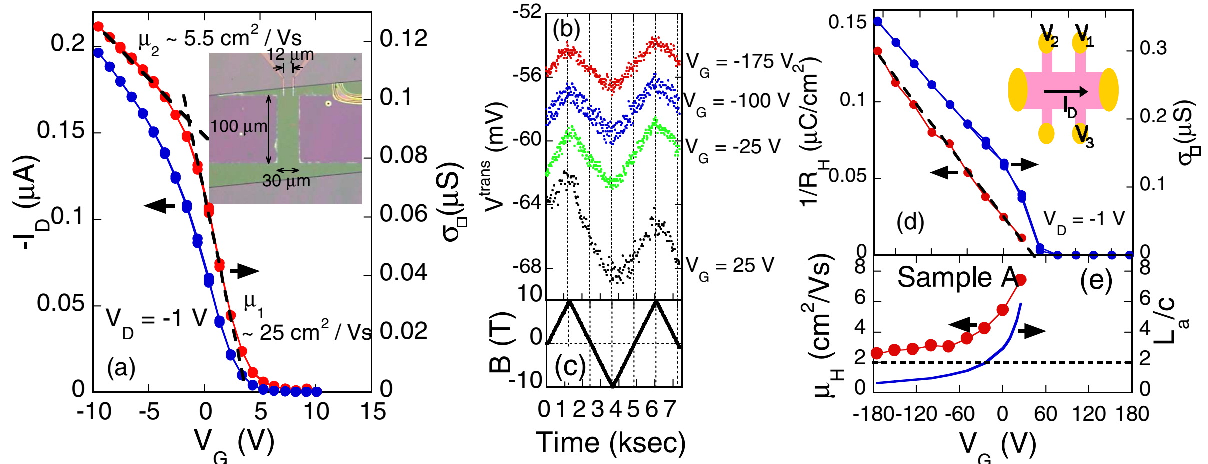

FIG. 1 (color online). (a) Transfer characteristics of a rubrene single-crystal field-effect transistor at 290 K. The red filled circles show the drain current and the blue filled circles show the four-probe sheet conductivity of the channel. The inset is a top view of the device. (b) Evolution of transverse voltage in the Hall-bar shaped rubrene single-crystal field-effect transistor (sample A) at 290 K for four different gate voltages from 25 to −175 V. Magnetic field is swept back and forth from −10 to 10 T perpendicular to the conduction channel, as shown in (c). (d) Inverse Hall coefficient (red filled circles) and sheet conductivity (blue filled circles) plotted as function of gate voltage at 290 K, for the Hall-bar shaped rubrene single-crystal field-effect transistor (sample A) illustrated in the inset. (e) Hall mobility as a function of gate voltage as a result of the simultaneous measurement of the Hall coefficient and the sheet conductivity of the same rubrene single-crystal field-effect transistor sample A (red filled circles) at 290 K. The blue solid line indicates a typical estimation of carrier-distribution depth with the unit of c-axis lattice constant of rubrene. The black dashed line shows the two-monolayer criterion for a guide.

polarization is absent in the gate dielectric layer. For the Hall-effect measurement, external magnetic field is slowly swept between 10 and -10 T back and forth to extract the field-dependent component from the evolution of transverse voltage V_{trans} ($\equiv V_3 - V_1$). Figure 1(b) shows V_{trans} of one sample (sample A) as a function of time in the magnetic fields B, changing as Fig. 1(c). Subtracting slightly drifting components by linear approximation, R_H is derived as $R_H = \Delta V_H/(I_D \Delta B)$, using the component of the Hall voltage ΔV_H, which varies concomitantly with B. The sign of R_H is positive, which is consistent with the hole accumulation in the rubrene crystals.

The inverse of the Hall coefficient is plotted in Fig. 1(d) together with $\sigma_\square$ as a function of gate voltage. In contrast to the nonlinear profile of $\sigma_\square(V_G)$, $1/R_H$ increases linearly in the region of $V_G < V_{\mathrm{th}}$. Moreover, the line of $C_i(V_G - V_{\mathrm{th}})$, which shows the charge amount modulated by the V_G application, well agrees with the $1/R_H - V_G$ profile. C_i is evaluated using ϵ_i and d_i of the PVP film; the former is defined by the ac impedance measurement and the thickness d_i is estimated to be 5 ± 0.5 μm with the laser optical microscope. The result means that $1/R_H$ indeed gives a good measure of the amount of carriers in the rubrene crystal, demonstrating extended electronic states that manifest themselves in significant wave function overlap. Similar conclusions were obtained in our previous report for the rubrene/SiO_2 FETs and by Podzorov *et al.* for air-gap rubrene transistors [11,14]. In addition, the linear increase of $1/R_H$ with V_G indicates absence of anomalous polarization of the gate dielectric layer, which guarantees correctness of Eq. (1). Therefore, the change in the slopes of the transfer curves is solely due to the significant V_G dependence of μ.

Hall mobility μ_H estimated by $R_H\sigma_\square$ gives average mobility of *mobile* carriers and is argued to give an intrinsic carrier mobility excluding influences of trapping events. μ_H is plotted as function of V_G in Fig. 1(e), showing that μ_H decreases rapidly with the negative V_G application. The result demonstrates nonequivalence of carriers introduced under different gate electric fields; neglecting electron correlation in such a low-carrier-density system, the $\mu_H(V_G)$ profile comes from variation of the mobility values depending on spatial distribution of the carriers. Under high gate fields, the carriers have tendency to distribute in the vicinity of the interface because of larger attractive electrostatic force and shorter screening length. Therefore, the result of Fig. 1(e) indicates that μ_H of the carriers located near the interface is reduced by significant scattering subjected to random potential on the amorphous polymers. On the other hand, carriers are more dilutely distributed into inner crystal because of more pronounced thermal diffusion against weaker gate field. Since diffusive bandlike transport is assumed in the above mechanism, we examine whether the mean free path ℓ can be sufficiently long with the maximum mobility of ~ 8 cm^2/V s in Fig. 1(e); within the nondegenerated electron gas model, ℓ can be evaluated at least ~ 7.5 Å at 300 K, assuming the effective mass of the holes m^* more than twice as large as the free electron mass [17]. As compared with the intermolecular distance b (~ 3.7 Å) in the stacking direction, ℓ is more than a few times longer, leaving a room to be reduced by additional scattering. When μ_H decreases down to ~ 2.5 cm^2/V s at higher gate voltage, the above simplified calculation gives ℓ comparable to b, so that the picture of the diffusive model becomes marginal. Since the maximum mobility in Fig. 1(e) is determined due to limitation of the measurement, even larger μ could be realized in the inner crystal. We note that bulk crystalline μ as high as ~ 35 cm^2/V s is reported for space-charge limited current at least in intensively purified pentacene crystals [8].

To have more microscopic ideas, one can employ a simple argument of the competition between the gate electric field to confine the carriers to the interface and their tendency to thermally diffuse into the crystal. We introduce a length scale L_a for the carrier distribution in the direction of thickness in the organic crystal, based on the Poisson's equation as discussed in Ref. [18]. L_a can be given as $\sim 2\epsilon_s k_B T/[eC_i(V_G - V_{\mathrm{th}})]$, where ϵ_s, k_B, and T are dielectric constant of rubrene in the thickness direction, Boltzmann constant and temperature, respectively. Assuming that $\epsilon_s \sim 3\epsilon_0$ (ϵ_0 is dielectric constant in vacuum) and that $V_{\mathrm{th}} \sim 50$ V, L_a is estimated for each V_G as shown in Fig. 1(e) by the unit of the lattice constant c in the direction of thickness. Since μ_H drastically varies as V_G with the carrier distribution of a few-monolayer thickness, the $\mu_H(V_G)$ profile in Fig. 1(e) can be viewed as a crossover from in-crystal to surface (a few-monolayer) carrier transport in the rubrene crystals. Therefore, the above simple estimation of L_a appears to be consistent with the present experiment, though more precise evaluation is needed to define the exact crossover point avoiding ambiguities of V_{th} and of the residual interface charge. The same discussion was also conjectured in some thin-film devices of field-effect mobility around 0.3 cm^2/V s though the intrinsic mobility was not given without Hall-effect measurement [19]. For pentacene thin films, similar charge profile is suggested as the result of *in situ* mobility measurement employing a layer-by-layer growth technique [20]. We also note that the highest room temperature mobility ~ 20 cm^2/V s achieved for the air-gap rubrene FETs is also with rather dilute carriers in the order of 10^{10} cm^{-2} [21], where the carriers are not conceived to be confined at the surface of the crystal.

Finally, we show temperature dependence of $\sigma_\square(V_G)$, $1/R_H(V_G)$, and $\mu_H(V_G)$ profiles in Fig. 2. Though the sheet conductivity and inverse Hall coefficient both apparently decreases with decreasing temperature, the overall temperature dependence of $\mu_H(V_G)$ is minor. Similarly prepared sample B shows near temperature independence of $\mu_H(V_G)$ with smaller range of the thermal cycle shown in Fig. 2(d), as the result of the compensation between the $\sigma_\square(V_G)$ and $1/R_H(V_G)$ profiles. It is not yet clear whether

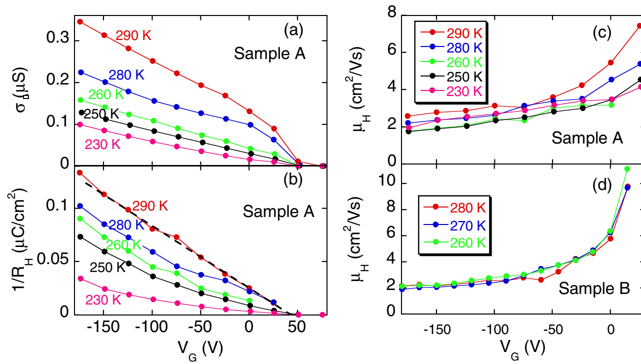

FIG. 2 (color online). (a) Four-probe sheet conductivity, (b) inverse Hall coefficient and (c) Hall mobility of the same rubrene single-crystal field-effect transistor (sample A) as shown in Fig. 3 at various temperatures. (d) Hall mobility of another similarly prepared rubrene single-crystal field-effect transistor (sample B) at various temperatures.

or not $\mu_H(V_G)$ can increase with decreasing temperature at the low-carrier-density limit as reported for the air-gap device with the density in the order of 10^{10} cm^2/V s [14], so that further idealization is required for the present PVP devices. Since effective surface trap levels increase in number at lower temperatures and partially terminate the applied gate electric field at the interface, the amount of the best mobile carriers located inside the crystal is reduced. As observed for the 230-K curve in Fig. 2(b), density of mobile carriers counted in $1/R_H(V_G)$ does not start to increase with negative V_G in the same rate as at room temperature, until the gate electric field mostly fills the band-tail states due to the trap levels around $V_G \sim -150$ V. At intermediate temperatures, admixture of the best mobile carriers ($\mu > 10$ cm^2/V s) deep in the crystal, moderately mobile carriers in the vicinity of the interface that are still counted in $1/R_H(V_G)$ ($\mu \sim$ 1–5 cm^2/V s), and surface trapped charge ($\mu \sim 0$ cm^2/V s), give rise to the complicated V_G dependence shown in Figs. 2(a) and 2(b).

It is to be emphasized that the present experiment first reports unambiguously that the carrier mobility inside the high-quality single crystals can be higher than that right at the interface in organic field-effect transistors, employing the Hall-effect measurements. The achievement of the near bulk carrier transport is due to thermal diffusion of the carriers into the crystal in the absence of dopant impurities, grounded on intrinsic-semiconductor character of the purified rubrene single crystal. We note that the situation is in sharp contrast to most inorganic devices on doped semiconductors, where the channels are confined to thin inversion layers. Since it was commonly believed that the carrier transport is always contaminated by the interfacial complexities in the organic FETs, the successful carrier doping into the "bulk" of the purified crystals is a marked experimental progress to offer a realistic prescription of designing high-mobility organic transistors, as well as to present genuine electronic systems induced in the molecular-orbital bands of neutral organic semiconductor crystals.

In conclusion, we found crossover from the high-mobility bulklike carrier transport to lower-mobility surface carrier transport, as the result of simultaneous measurements of conductivity and the Hall effect as holes are accumulated up to $\sim 10^{12}$ cm^{-2}. High-quality rubrene single-crystal/PVP field-effect transistors are prepared with minimized trap densities at the interface so that the gate electric field can penetrate into the crystal. As the result, diffusive bandlike transport is realized in the inner crystal with reduced scattering rate away from the interface complexity. Interestingly, the above mechanism to achieve the high mobility is practically applicable to real FET devices, because of intrinsic-semiconductor character of the organic semiconductors which allows thermal diffusion of the induced carriers. The method of evaluating bulk mobility at weak gate electric fields will be useful also in developing high-mobility organic materials.

We thank helpful discussion with A. Morpurgo. This study was partially supported by a Grant-in-Aid for Scientific Research (No. 17069003, and No. 18028029) from MEXT, Japan and Industrial Technology Research Grant Program in 2006 from NEDO, Japan.

*Electronic address: takeya@chem.sci.osaka-u.ac.jp

[1] M. Pope and C. Swenberg, *Electronic Processes in Organic Crystals and Polymers* (Oxford University, Oxford, 1999), 2nd ed..
[2] *Organic Molecular Crystals* (Springer-Verlag, Berlin, 1980).
[3] V. M. Kenkre *et al.*, Phys. Rev. Lett. **62**, 1165 (1989).
[4] V. Podzorov *et al.*, Phys. Rev. Lett. **93**, 086602 (2004).
[5] A. Troisi *et al.*, Phys. Rev. Lett. **96**, 086601 (2006).
[6] N. Karl in *Organic Electronic Materials: Conjugated Polymers and Low Molecular Weight Organic Solids*, edited by R. Farchioni and G. Grosso (Springer, New York, 2001).
[7] W. Warta *et al.*, Appl. Phys. A **36**, 163 (1985).
[8] O. Jurchescu *et al.*, Appl. Phys. Lett. **84**, 3061 (2004).
[9] V. Y. Butko *et al.*, Phys. Rev. B **72**, 081312 (2005).
[10] V. Podzorov *et al.*, Appl. Phys. Lett. **82**, 1739 (2003).
[11] V. Podzorov *et al.*, J. Appl. Phys. **94**, 5800 (2003).
[12] R. W. I. de Boer *et al.*, Appl. Phys. Lett. **83**, 4345 (2003).
[13] J. Takeya *et al.*, Jpn. J. Appl. Phys. **44**, L1393 (2005).
[14] V. Podzorov *et al.*, Phys. Rev. Lett. **95**, 226601 (2005).
[15] J. Takeya *et al.*, Appl. Phys. Lett. **85**, 5078 (2004).
[16] I. Yagi *et al.*, Appl. Phys. Lett. **84**, 813 (2004).
[17] ℓ is estimated as $\sim\sqrt{3k_BTm^*}(\mu/e)$ at 300 K.
[18] G. Horowitz *et al.*, J. Appl. Phys. **87**, 4456 (2000).
[19] J. A. Merlo *et al.*, J. Am. Chem. Soc. **127**, 3997 (2005).
[20] M. Kiguchi *et al.*, Phys. Rev. B **71**, 035332 (2005).
[21] E. Menard *et al.*, Adv. Mater. **16**, 2097 (2004).